JOURNAL OF PROPULSION AND POWER
Vol. 33, No. 2, March–April 2017

Spacecraft-Charging Characteristics Induced by the Operation of Electrospray Thrusters

Fernando Mier-Hicks* and Paulo C. Lozano†
Massachusetts Institute of Technology, Cambridge, Massachusetts 02139

DOI: 10.2514/1.B36292

Theoretical and experimental methods were developed to investigate the charging characteristics anticipated to be observed on spacecraft during the operation of electrospray thrusters. These devices produce positively and negatively charged particles of similar mass and velocities. An electrical model of this configuration was created to predict the charging properties of electrically isolated systems. This model simulates a bipolar electrospray-thruster system. Experiments were conducted on a test bed, in which a mock-up satellite is magnetically levitated inside a vacuum chamber. The mock-up is equipped with batteries, power conditioning, radio transmitter, and electrospray thrusters. The results from the experimental tests demonstrate that neutralization with heavy ionic species is indeed possible. The thrusters are able to fire in a bipolar configuration for long periods of time inducing bounded spacecraft charging in the range from −400 to +600 V when emitting currents of about 20 μA. It was found that the presence of low-energy ions produced by the fragmentation of large clusters plays a significant role in the neutralization characteristics. This electrical model was verified by reproducing the experimental results, thus validating its use to estimate bulk spacecraft-charging properties.

Nomenclature

A, B	=	exponential emission model parameters
B	=	intercepted current fraction
$\bar{F}$	=	nominal thrust
$\bar{F}_b$	=	nominal bipolar thrust
$\bar{F}_*$	=	net thrust taking into account charging effects
$\bar{F}_{*b}$	=	net bipolar thrust taking into account charging effects
f_{eng}	=	interpolation function used to approximate ion-beam-energy distribution
I_{em}	=	thruster emitted current
I_{out}	=	current that makes it out of the extractor
I_{return}	=	current that returns to the satellite
I_{sp}	=	specific impulse
I_{thr}	=	current that contributes to net thrust
q/m	=	charge-to-mass ratio
R	=	quadratic emission model parameter
V_{HV}	=	potential of the high-voltage power supply with respect to the high-voltage return node
V_{HVGround}	=	potential of the high-voltage return node with respect to satellite ground
V_{Sat}	=	potential of the satellite with respect to external environment
V_{str}	=	thruster startup voltage
V_{Th}	=	potential between emitter and extractor

I. Introduction

ELECTROSPRAY thrusters are a type of electric-propulsion device for spacecraft that work by emitting positively or negatively charged particles from an electrically conductive liquid by means of a high electrical field. The specific nature of emitted charges depends on the thruster's operational characteristics and the type of liquid used. When room-temperature ionic liquids are used, the emission typically consists of molecular ions and/or small ion clusters [1]. Room-temperature ionic liquids are molten salts that remain in the liquid phase at ambient temperature. These substances are composed of positive and negative ions, with no intervening solvent and exhibit zero vapor pressure, thus allowing their use in space without concerns of evaporation. Ions are expelled from the device at high velocities generating thrust with a high specific impulse. The emission of charged particles from this and other types of electric thrusters plays a fundamental role in how the potential of the spacecraft varies with respect to the local environment or within different parts of the vehicle. It is important to predict and control the charging characteristics to prevent a decrease of performance, or even damage to payloads and subsystems.

To achieve ionic emission, large electric fields on the order of 1 V/nm are required on the surface of the liquid [2]. To reach such field magnitudes, sharp emitter structures capable of transporting the liquid are used. A voltage difference is applied between the conductive liquid and a downstream extractor electrode aperture, as shown in Fig. 1. The potential difference produces instability on the liquid surface, which shapes it into a sharp meniscus. At the apex of this meniscus, the field is intensified to the values required for ion emission. These ions are then accelerated by the same electric field that extracted them from the ionic liquid. Ions that successfully pass through the extractor generate net thrust for the spacecraft. Because of their inherently small scale, electrospray thrusters are attractive as a propulsion technology for small satellites. In addition, because they are modular, they are also scalable to larger spacecraft classes.

Each electrospray-emission site generates tens to hundreds of *nanoamperes* in ionic current with velocities in the kilometer-per-second range, and produces tens of nanonewtons of thrust [3]. Larger thrust is obtained when operating a large number of emitters in a parallel array configuration.

Several array configurations utilizing microfabrication techniques have been proposed [4–7]. In this study, ion electrospray propulsion systems (iEPSs) are used. These thrusters are developed at the Space Propulsion Laboratory at the Massachusetts Institute of Technology [5], and schematically depicted in Fig. 2.

The thruster arrays are housed in a silicon frame that has dimensions of 13 × 12 × 2.4 mm. The frame contains a porous glass emitter substrate holding 480 laser-ablated tips. Above these tips sits a gold-coated silicon extractor grid. Emitted ions move through the apertures in the grid to the outside environment. The array produces about 0.1 μN of thrust per microampere of emitted current. The arrays used in this study operate nominally around 150 μA of current, which translates into ~15 μN of thrust per thruster. The propellant

Received 18 April 2016; revision received 12 July 2016; accepted for publication 25 July 2016; published online 27 October 2016.

*Ph.D. Candidate, Department of Aeronautics and Astronautics, 77 Massachusetts Ave.; ferhicks@mit.edu.

†Professor, Department of Aeronautics and Astronautics, 77 Massachusetts Ave. Member AIAA.

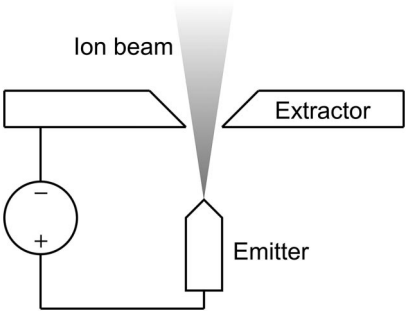

Fig. 1 Electrospray single emitter.

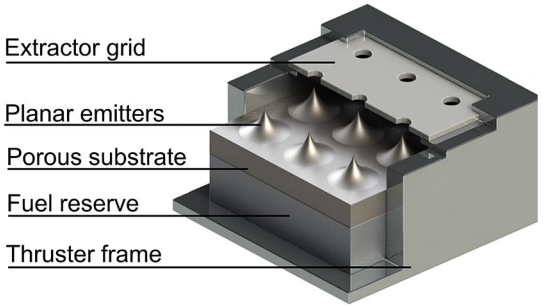

Fig. 2 Electrospray-thruster concept.

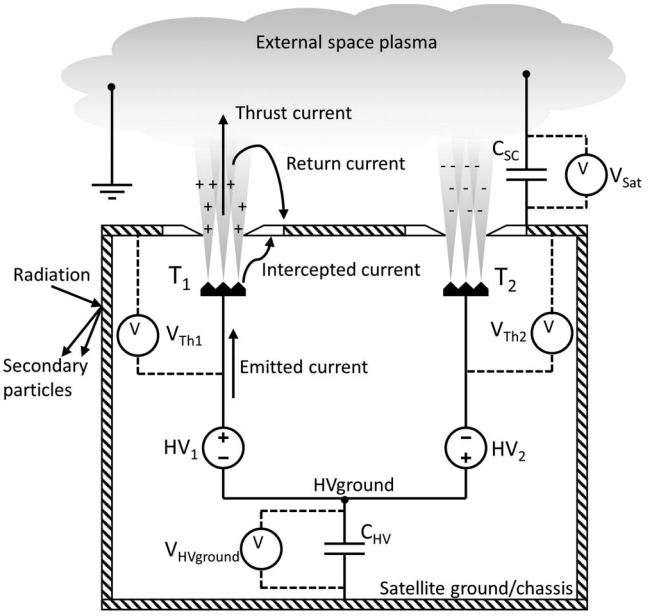

Fig. 3 Bipolar configuration for electrospray thrusters.

used travels from a fuel reserve by capillary action. Including this reserve, each iEPS module has dimensions of $14 \times 14 \times 14$ mm.

Spacecraft charging occurs when there is an imbalance of electric currents from the spacecraft to the environment. In space, the environment is usually low-density and low-temperature plasma, which interacts electrically with the satellite. Electrons and positive ions present in the plasma can collide with the spacecraft and deposit their charge. At the same time, backscattered and secondary particles are leaving the spacecraft and carrying their charge with them. Finally, radiation (photon or otherwise) produces secondary emission of particles when intercepted by the spacecraft. In a noncharging scenario, all these currents balance out and the satellite remains with a constant charge. Current imbalances cause the net charge on the satellite to increase positively or negatively. If an electric-propulsion device were to continuously emit a positively charged ion beam, the satellite may charge sufficiently negative to prevent emitted ions from escaping the spacecraft. The ions that return generate no net thrust. For this reason, plasma-based electric-propulsion devices, such as ion engines and Hall thrusters, neutralize their positively charged ion beams.

The neutralization of the beam is typically done via an external cathode, which is, in its simplest form, an electron gun. Cathodes are an integral part of these types of thrusters; they have a large influence on the lifetime and performance of the device. Because electrons are much more mobile than ions, the neutralization dynamics of plasma thrusters occur as fast as the characteristic charging time. Although early anxiety surrounded the possibility of effectively neutralizing these devices, now it is well known that electron-emitting cathodes work for this purpose [8,9].

Just as in ion engines, electrospray thrusters are electrostatic devices that use electric fields to accelerate charged species. However, they possess a key difference with respect to plasma propulsion devices: electrospray thrusters can accelerate positive or negative ions of similar mass, generating either a positive or negative ion beam, potentially eliminating the need for an external cathode. If two separate electrospray thrusters are fired in such a way so one provides a positive ion beam and the other an identical negative ion beam, then the spacecraft should not charge.

The bipolar mode of operation raises important questions, mainly the implications of the different properties between highly mobile electrons and negative ions. The electrospray bipolar arrangement is shown in Fig. 3. Note that the extractors of both thrusters are electrically connected to the satellite ground or chassis. When electrospray thrusters are fired, the polarity of ions being extracted is periodically alternated to avoid electrochemical reactions that could degrade the emitter tips [10]. The power processing unit (PPU) generates the high voltage needed to achieve emission and also alternates its polarity every ~30 s.

There are certain processes that should limit the potential that a spacecraft can reach while operating electrospray thrusters in a bipolar configuration. These processes act as self-regulating mechanisms that ensure emission can proceed even with differences in emission profiles between thrusters. A key aspect that allows these self-regulating mechanisms to occur is the galvanic isolation between the high-voltage return, HV_{Ground}, and the spacecraft ground provided by the C_{HV} capacitor; see Fig. 3.

The current emitted by an electrospray thruster has approximately a quadratic dependence on the applied voltage once a threshold voltage is surpassed. The threshold value is usually referred to as the startup voltage. Because of the nonzero divergence of the ion beam, a portion of the emitted current is intercepted by the extractor. This intercepted current is usually <5% of the emitted current [5]. The current vs voltage (I-V curve) characteristic of a typical iEPS device is shown in Fig. 4.

Because of manufacturing tolerances, no two thrusters are identical, which means that each thruster has a similar but unique I-V curve. In the case that two nonidentical thrusters are fired in the bipolar configuration at a constant voltage, one of them will emit more current than its counterpart. Additionally, due to manufacturing variability, some tips are sharper and closer to the extractor, which reduces the startup voltage for that specific device.

Suppose that thruster T_1 in Fig. 3 emits slightly more current at a given voltage than thruster T_2. Once emitting, the difference in currents will charge C_{HV} negatively, shifting HV_{Ground} to a negative potential with respect to the satellite ground and, therefore, the extractors. Because the thruster-voltage sources are constant, the potential differences between the thruster tips and the extractor, V_{Th1} and V_{Th2}, become more negative. The reduction in potential causes thruster T_1 to emit less positive ions and T_2 to emit more negative ions. This effect tends to balance the emitted currents, reaching equilibrium when both positive and negative emitted currents are identical. When the equilibrium is reached, C_{Hv} stops charging and $V_{HVGround}$ is nonzero.

Ideally, C_{HV} could have a capacitance of zero, but, in reality, a finite capacitance is needed to reduce the amount of noise produced by rapid changes in $V_{HVGround}$, increasing PPU performance. For this

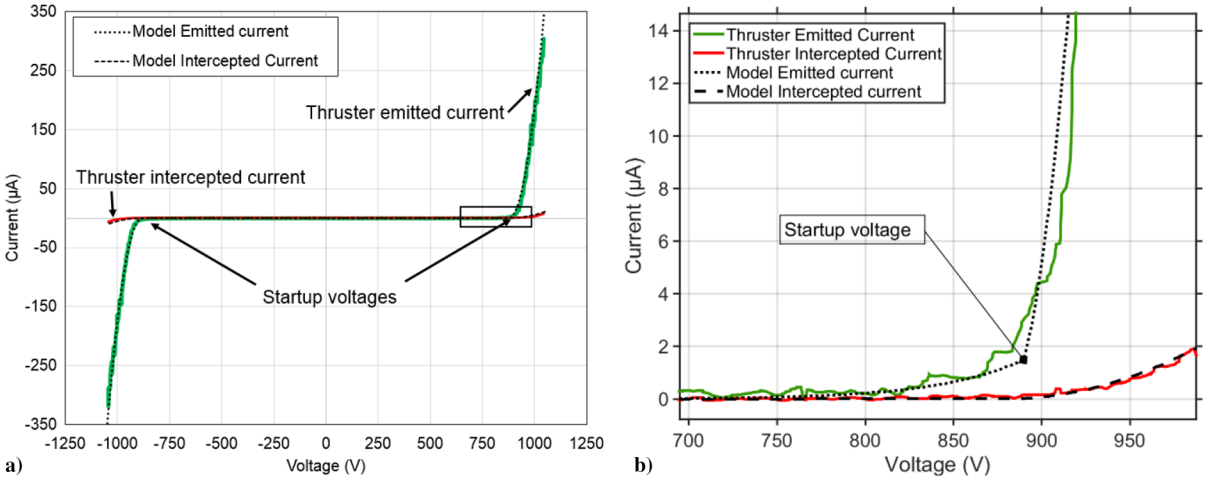

Fig. 4 Experimental *I-V* curve compared to the electrical model: a) complete emission profile and b) detailed region bounded by the box in a).

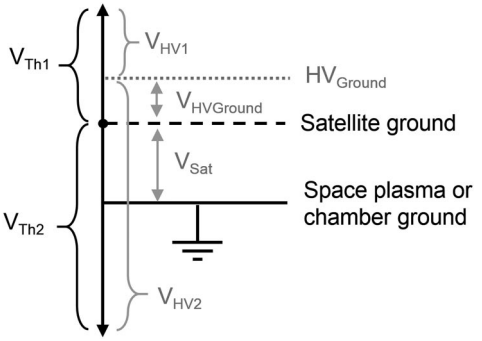

Fig. 5 Relevant potentials in the bipolar configuration for two dissimilar thrusters.

reason, a capacitance of 0.1 μF to 10 nF was used in simulations and experiments.

In Fig. 5, a summary of the different potentials in the bipolar configuration is shown. It is important to notice the distinction between the power-supply voltages, V_{HV1} and V_{HV2}, and the thruster voltages, V_{Th1} and V_{Th2}. If $V_{HVGround}$ is zero, then the thruster voltages would become identical to the power-supply voltages.

Electrospray thrusters are known to emit not only single ions, but also ions attached to a certain number of neutral pairs [1,11]. The fraction of solvated ions with respect to single ions can reach 30% or more in some cases [12,13]. Some of these solvated ions are known to fragment during and after acceleration.

A dimer (defined as $n = 1$) can separate into a pure ion and a neutral in a fragmentation event. If the fragmentation occurs outside of the thruster, the ion and neutral will travel at the same velocity as before, but they will be no longer attached. The fragmented ion would then have less energy compared to a single ion that was accelerated to the full thruster potential. When the spacecraft charges up, some ions will be electrostatically attracted to the satellite, whereas ions of opposite polarity will be repelled. If the potential of the spacecraft is larger than the energy of an attracted ion, it will slow down, stop, and return to the spacecraft. When the ion collides with the spacecraft, it will deposit its charge, thus reducing the satellite charging rate. The ion collision could also create secondary particles that are repelled by the spacecraft and aid in neutralization. Interestingly, for electrospray thrusters, low-energy ions born from fragmentation events would return more readily. In the bipolar configuration, the returning ions enable the spacecraft potential to remain significantly lower than the full ion acceleration voltage applied to the thruster.

II. Electric Model

The charging behavior of a spacecraft equipped with electrospray thrusters can be modeled with real and virtual capacitors connected to different parts of the satellite and the outside environment. A schematic of such a model is shown in Fig. 3. The circuit is simulated in a SPICE electronics package (MultiSim). Passive elements are used to model the complete system, except for the thrusters, which are represented by a set of current sources controlled by nonlinear expressions. The current sources are connected, as shown in Fig. 6.

The difference between emitted and intercepted currents that makes it out of the thruster is referred to as the *out current*. A portion of the out current could be forced to return to the extractor if the spacecraft potential is nonzero. Low-energy ions that are produced by a spontaneous, metastable fragmentation event would be the first contributors of this *return current*. The current that is able to exit the thruster and does not return to the spacecraft is referred to as the *thrust current*. The thrust current is simply the emitted current minus the intercepted and return currents.

The space-plasma flux, radiation-induced currents, and secondary particle generation could be represented by a series of nonlinear-equation-driven current sources. These current sources only become relevant when their magnitude is on the order of the differential intercepted currents. At a nominal operation point, the thrusters emit 150 μA; the maximum differential intercepted current at this point is in the order of 7.5 μA [5].

For example, of a 1 U CubeSat with a surface area of 0.006 m^2, orbiting at an altitude of 500 km, and a large positive potential (~50 V) with respect to the space plasma, the electron saturation current would be around 6 μA at solar maximum [14,15]. For the

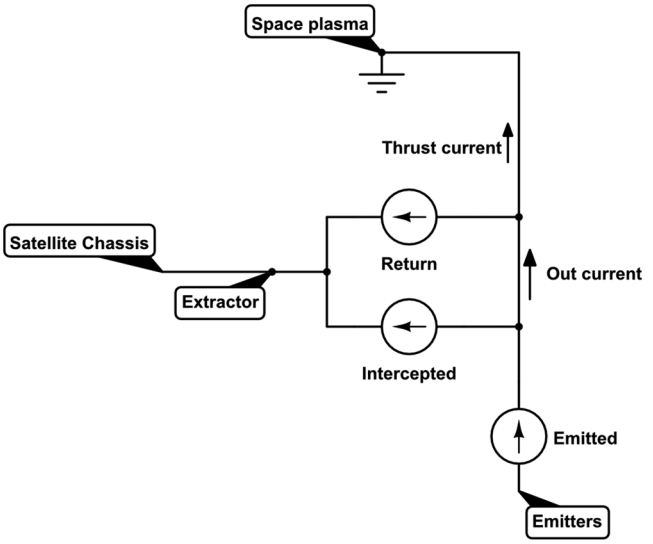

Fig. 6 Current network configuration for the electrospray-thruster model.

same satellite now charged to −50 V, the ion-saturation current is ∼0.14 μA. The space-plasma density decreases with higher altitudes. Because the collected electron and ion fluxes are proportional to the plasma density, higher orbits will yield a smaller electron and ion-saturation currents.

The electric model described in this work does not include plasma currents, which is a realistic approximation for satellites orbiting above 500 km. For orbits below 500 km, the ion-saturation current is still negligible, but the electron saturation current has a significant effect. The model attempts to approximate experiments conducted on the ground in which no plasma source was present.

A. Emitted and Intercepted Current Modeling

With normal electric fields in the range of 1–2 V/nm, individual ions are extracted from the ionic liquid by field emission [1]. After this threshold is achieved, field emission increases exponentially with the electric field [16]. Field emission continues until the ion transport to the apex of the tip is limited by the ionic liquid conductivity [16]. After this regime, the emission current presents a linear dependence with applied voltage for a single emission site. Guerra-Garcia et al. show that not all the tips in the thruster emit ions at the same potential [17]. The number of activated tips with increasing voltage can be approximated, to first order, as a linear relationship. The emission behavior after the exponential field-emission regime can be approximated as a quadratic function.

A patched model is used to model the emission behavior. For voltages lower than the startup voltage, the emission behavior is approximated with an exponential relationship. For voltages higher than the startup voltage, a quadratic approximation is used. The two approximations meet at the startup voltage and provide a smooth transition.

The exponential model is controlled by two parameters, A and B, which relate to the activation energy of the process and other physical constants. Two parameters control the quadratic emission profile: the startup voltage V_{str} and a constant factor that controls the steepness R. Equation (1) shows the piecewise function that defines the thruster current vs voltage relation used in the electrical model. It only incorporates positive emission; the negative emission is obtained by simply inverting the emitted-current sign.

$$I_{em}(V_{Th}) = \begin{cases} AV_{Th}(e^{B\sqrt{V_{Th}}}), & v \le V_{str} \\ \frac{(V_{Th}-V_{str})^2}{R}, & v > V_{str} \end{cases} \tag{1}$$

The parameters in the model are fitted from experimental data. Positive- and negative-emission asymmetries could be modeled with slightly different parameters for each polarity. In this work, positive and negative emissions are taken to be symmetrical. The interception current is modeled as a fixed fraction, β, of the emitted current:

$$I_{intercepted} = \beta I_{emitted} \qquad 0 < \beta < 1 \tag{2}$$

Figure 4 shows the similarity between the emission profile of the model and the experimental data. With respect to the experimental data, the emitted and intercepted current models have an R^2 value of 0.97 and 0.99, respectively.

B. Return-Current Modeling

A retarding potential analyzer (RPA) can be used to extract the energy distribution of an ion beam [5,18]. A representative RPA curve of an electrospray thruster fueled with EMI-BF4 emitting positive ions is shown in Fig. 7 [5]. Because of the similarity of positive- and negative-emission energy distributions for a thruster fueled with EMI-BF4, the positive RPA curve in Fig. 7 is taken as a representative distribution for both polarities. A linear piecewise interpolation table, $f_{eng}(V_{Sat})$, is used to fit the return-current model to the specific experimental data. The return current becomes nonzero when the spacecraft potential is nonzero and opposite in polarity with respect to the emitted current. When these conditions are met, the lookup-table function is used to calculate the total return-current fraction using Eq. (3) and Table 1. In this model, the extractors

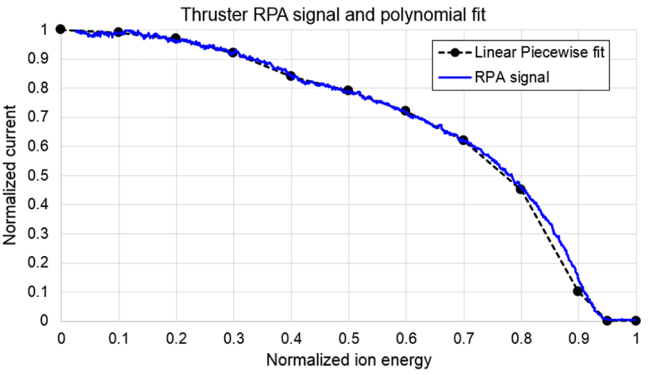

Fig. 7 RPA curve of an iEPS fueled with EMI-BF4 and firing in positive mode.

are directly connected to the satellite chassis, which is also satellite ground. The external environment is taken as the global ground.

$$I_{return}(V_{sat}) = \begin{cases} 0, & V_{sat} = 0 \\ 0, & V_{sat} > 0, \quad I_{em} > 0 \\ 0, & V_{sat} < 0, \quad I_{em} < 0 \\ I_{out}[f_{eng}(V_{sat})], & \text{All other } V_{sat} \end{cases} \tag{3}$$

III. Effects of Charge on Thrust

The nominal thrust $\bar{F}$ of an electrospray thruster can be approximated by [19]

$$\bar{F} = I_{thr}\sqrt{\frac{2V_{Th}}{(q/m)}} \tag{4}$$

the charge-to-mass ratio of the expelled ions is (q/m), and I_{thr} is the thrust current. Courtney et al. [19] and Courtney and Shea [20] have shown that numerical factors can be applied to V_{Th} and (q/m) to account for different degrees of solvation in the emitted ions and energy dispersion in the beam.

In the bipolar configuration, a nonzero satellite potential will modify the nominal thrust by repelling one ion beam and attracting the opposite-polarity ion beam. The thrust contribution of the polarity being attracted will be reduced, whereas the one being repelled will be increased. The thrust that takes into account these charging effects, $\bar{F}_*$, is then calculated by introducing the potential of the satellite, V_{Sat}, into Eq. (4), resulting in Eq. (5).

$$\bar{F}_* = I_{thr}\sqrt{\frac{2(V_{Th}+V_{sat})}{(q/m)}} \tag{5}$$

An expression for the fractional change of the thrust with reference to its nominal value can then be obtained:

Table 1 Lookup table used to fit RPA curve

Normalized ion energy	Normalized current
0	1
0.1	0.99
0.2	0.97
0.3	0.92
0.4	0.84
0.5	0.79
0.6	0.72
0.7	0.62
0.8	0.45
0.9	0.1
0.95	0
1	0

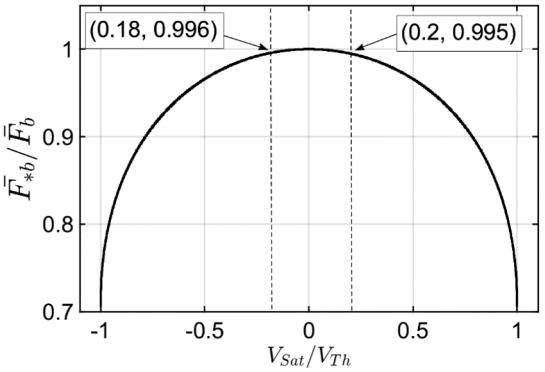

Fig. 8 Effects of satellite potential on thrust; the two coordinates represent the satellite-potential boundary measured for the test described in Fig. 18.

$$\frac{\bar{F}_*}{\bar{F}} = \sqrt{1 + \frac{V_{\text{sat}}}{V_{\text{Th}}}} \tag{6}$$

Applying this relation to the bipolar configuration, in which two thrusters are fired, and normalizing by twice the nominal thrust, $\bar{F}_b$, result in the bipolar-thrust fractional change, $\bar{F}_{*b}/\bar{F}_b$:

$$\frac{\bar{F}_{*b}}{2 \cdot \bar{F}} = \frac{\bar{F}_{*b}}{\bar{F}_b} = \frac{\sqrt{1 + \frac{V_{\text{sat}}}{V_{\text{Th1}}}} + \sqrt{1 + \frac{V_{\text{sat}}}{V_{\text{Th2}}}}}{2} \tag{7}$$

Assuming V_{Th1} is positive and V_{Th2} is identical in magnitude but negative, it is possible to graphically observe the effect of charge on thrust, Fig. 8.

As expected, when the satellite potential is zero, the pair of thrusters produces twice the nominal thrust of a single thruster. When the potential of the satellite deviates from zero, the thrust is less than $\bar{F}_b$, with a square-root dependence. In the worst-case scenario, when the satellite fully charges to one of the thruster potentials, the total thrust would be 70% compared to the noncharged case. Even though the species of the different ion beams are being repelled and attracted by the same potential, the effect goes as the square root of the satellite potential. Therefore, the increase in thrust by the repelled ion beam is not sufficient to counteract the reduction in thrust by the attracted ion beam. The vertical dashed lines in Fig. 8 show the charging envelope for the experimental test to be described in Sec. V.D. As seen in the following sections, such envelope is representative of spacecraft-charging experiments. Consequently, it is anticipated that charging will have an, albeit small, nonzero effect on thrust.

IV. Maglev Test Bed

A magnetically levitated test bed was used to study the charging characteristics of electrospray thrusters. This instrument levitates a mock-up satellite using magnetic fields inside a vacuum chamber, which electrically isolates the satellite from the chamber. The mock-up satellite is very similar to a CubeSat, with dimensions of 5 in. per side. The levitated satellite is equipped with batteries, computer, radio, PPU, and thrusters. Although magnetically levitated and under vacuum, the satellite can rotate freely around a single zero-friction degree of freedom. The thrusters are then fired remotely, causing the satellite to rotate. The movement can then be analyzed and thrust calculated. A charge sensor is placed in close proximity to, but not contacting, the levitated satellite to measure its charge in real time. The electrical ground in this test bed is considered to be the chamber metal wall and the test-bed frame, see Fig. 9. The pressures reached inside the vacuum chamber for all tests were lower than 5×10^{-6} torr. More information on the test bed can be found in [21–23].

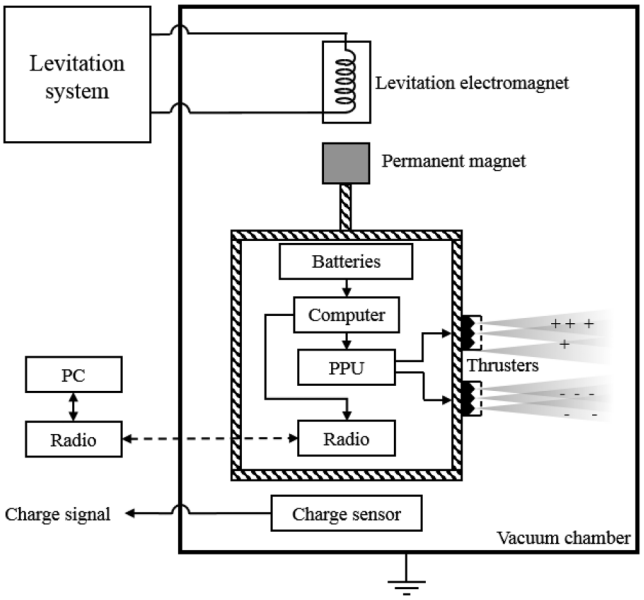

Fig. 9 Maglev test-bed schematic.

A. Power Processing Unit

The PPU in the satellite provides telemetry of emitted and intercepted currents, and thruster voltage. The telemetry is sampled at 10 Hz. All telemetry is filtered by the PPU circuitry with a resistor-capacitor (RC) filter that reduces signal noise, improving PPU performance. The RC filters used have a cutoff frequency of 1.6 kHz. The filters add certain lag on the monitored signals, visible in Figs. 10a and 10b. The emitted and intercepted current circuitries have a measured uncertainty of ± 3 μA. The voltage circuitry has a measured uncertainty of ± 5 V.

B. Charge Sensor

A parallel-plate capacitor was designed and integrated into the test bed, and used as a noncontact charge sensor. The levitating satellite acts as one plate, whereas a shielded metal disk acts as the other. The shielded metal disk is placed in close proximity to the bottom metallic face of the levitated satellite. When the satellite charges, it induces a mirror charge on the shielded metal disk, which is then measured by a high-impedance electrometer, see Fig. 11. A Keithley 6514 digital electrometer was used to perform this measurement.

The disk is shielded to avoid unwanted sources of charge that could be collected by the sensor plate. The shield is composed of a metallic housing that is grounded and covers the inner disk from all sides except the top one, used for measuring. The wire used to carry the sensor-plate signal is a shielded coaxial cable grounded to the chamber. The charge-sensor plate has a diameter of 68.6 mm and sits 3 mm below the levitated satellite.

The charge sensor is calibrated by biasing the levitating satellite to several known potentials with an external high-voltage power supply. The calibration approach exploits the fact that knowing the satellite potential is more relevant than measuring the amount of coulombic charge the satellite has. The procedure generates a linear transfer function of the satellite potential vs the measured mirror charge on the sensor plate; see Fig. 12. The linear fit has a correlation coefficient of 0.99.

The orientation and distance of the levitated satellite with respect to the sensor plate affect the capacitive coupling of the device. Any movement of the levitated satellite therefore reduces charge-sensor performance. The effect of movements on the measured satellite potential can be observed when the satellite is rotating with a constant speed and no thrusters are active, Fig. 13. Taking into account the error introduced by satellite movement, as shown in Fig. 13, the uncertainty of the charge sensor is estimated to be ± 10 V. Tests described in later sections have charging levels of around ± 800 V. The uncertainty of the charge measurement in these cases is then 1.25%.

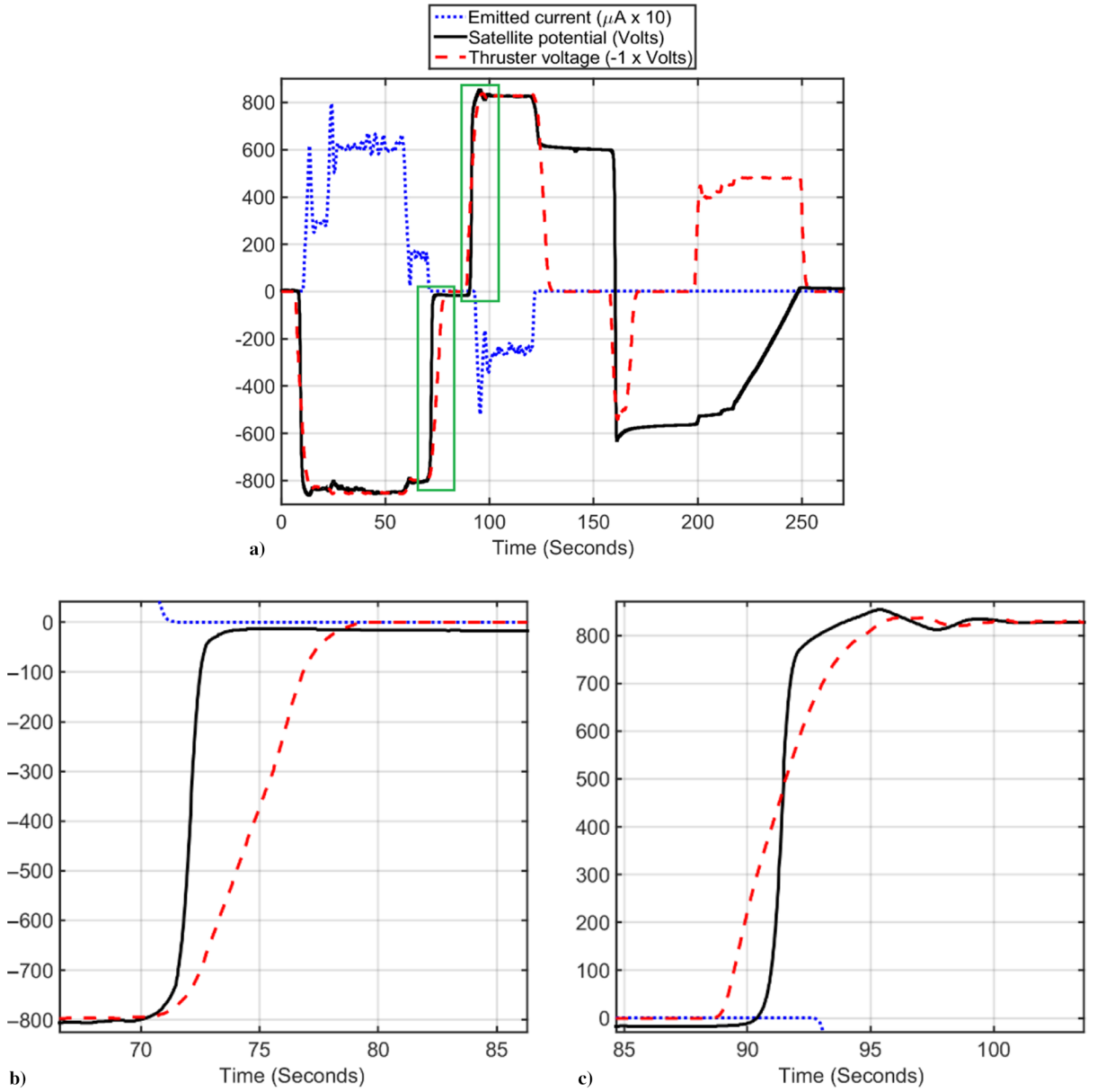

Fig. 10 Results of single electrospray-thruster test in maglev test bed: a) complete test, b) detailed view of the turnoff transient shown in the leftmost box region of a), and c) detailed view of the turn-on transient shown in the rightmost box region of a).

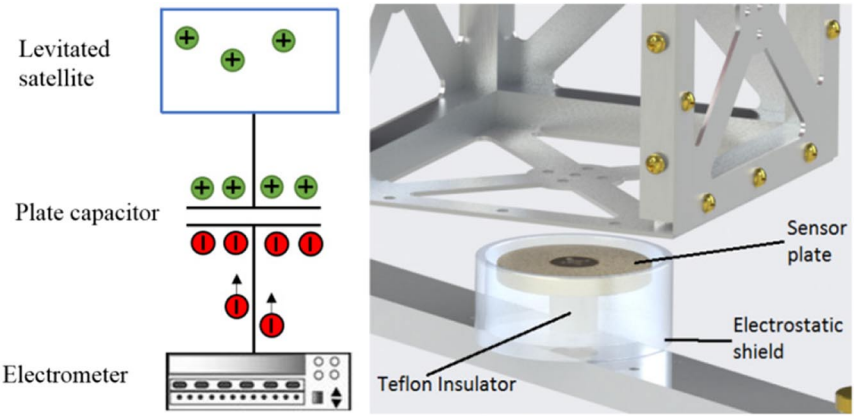

Fig. 11 Charge-sensor concept and construction.

V. Results

A. Electric Model

The circuit simulated is identical to the one in Fig. 3, in which the thruster model is composed of the current-source network shown in Fig. 6. The potential of the high-voltage power-supply return, HV_{Ground}, with respect to the satellite will be referred to as $V_{HVGround}$. The potential at which the satellite floats with respect to the external plasma will be referred to as satellite potential or V_{Sat}. In this specific

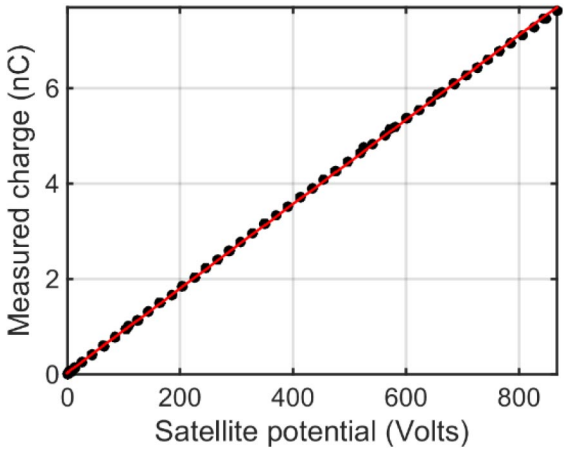

Fig. 12 Transfer function of charge sensor with linear fit.

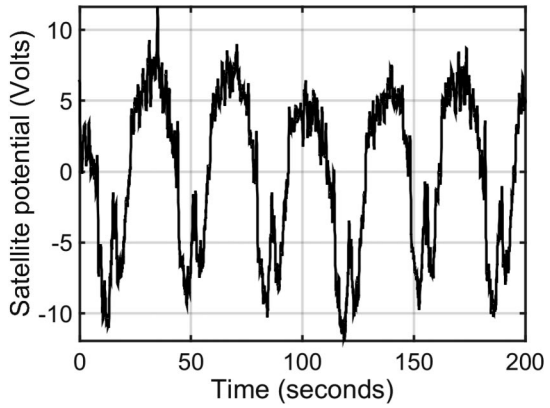

Fig. 13 Measured satellite potential while satellite is rotating at 1.7 rpm with no thruster emission.

simulation, the capacitances of C_{HV} and C_{SC} are chosen to make charging effects apparent in the timescales presented, slower than in reality. Similarly, the steepness factor R of the thruster model is chosen to aid in the visualization of the data. The voltage applied to the thrusters is a bipolar 1000 V square wave that simulates polarity switching with a switching time of 500 ms.

In this simulation, a higher startup voltage was chosen for T_2 along with a higher interception fraction compared to T_1. The asymmetry in emission profiles will make charging effects evident. The results of the simulation, as well as the model parameters, are shown in Fig. 14 and Table 2, respectively.

Because of the asymmetry in the emission profiles, T_1 emits more current, with less interception at any given thruster voltage compared to T_2. At time 50 ms, in Fig. 14, the potential across T_1 surpasses its startup voltage and starts emitting. At this same instant, the potential across T_2 is not high enough and is still in the exponential part of its I-V curve.

Table 2 Thruster-model parameters used for simulation

	Parameter	Value	Units
T_1	V_{str}	800	V
	A	1.075×10^{-24}	V^{-1}
	B	1.173	$V^{-1/2}$
	R	1.074×10^{8}	Ω^2
	β	1	%
T_2	V_{str}	850	V
	A	1.075×10^{-24}	V^{-1}
	B	1.173	$V^{-1/2}$
	R	1.074×10^{8}	Ω^2
	β	10	%
	C_{SC}	50	pF
	C_{HV}	100	nF

The positive charge expelled from T_1 forces C_{SC} to negatively charge with respect to global ground. The current imbalance also forces C_{HV} to negatively charge with respect to the satellite. The potential in C_{HV} shifts the thruster voltages negative. Once the potential across T_2 reaches its startup voltage, it starts emitting negative ions. There is now less of a difference in emitted currents, which slows down the rate at which the satellite charges, time 90 ms. As C_{HV} negatively charges, the potential difference across T_2 becomes greater and the potential difference across T_1 becomes smaller. This shift in thruster potentials forces T_2 to emit more current and T_1 to emit less current. The quadratic relationship between the emitted current and the thruster potential makes a difference of only a few volts very significant on the emission current. Therefore, C_{HV} only has to charge a few tens of volts to balance the emission currents. The overshoots of the emitted currents visible at times 50 and 550 ms are caused by this noninstantaneous charging of C_{HV}. While C_{HV} charges, the emitted currents are not identical. Eventually, C_{HV} charges to the potential that shifts the thruster power supply enough to make both emitted currents the same. Despite this equilibrium, there could still be differences in the amount of intercepted currents being collected by the extractors from each thruster. In this simulation, the difference in intercepted currents is due to the different interception fractions assigned to each thruster.

The charging produced by the differential interception fraction of the thrusters will be mitigated by the return current. For instance, at time 300 ms in Fig. 14, well beyond the transients induced by C_{HV} charging, the emitted currents are balanced. The interception fraction of T_2 is 10 times larger than T_1; therefore, the extractors are collecting a net negative current. The negative current charges the satellite to a negative potential, forcing the return of positive ions from T_1, which eventually slows the rate of satellite charging. In this example, the satellite potential stabilizes at -600 V due to the positive return current from T_1 being the same as the differential intercepted current. Using the RPA curve in Fig. 7, it can be estimated that only 30% of the ions ejected by the thruster have energies less than 60% of the thruster potential. If the ion beam had higher energy dispersion with ions of lower energy, the equilibrium potential would be smaller. In a similar way, if the beam were truly monoenergetic, the equilibrium potential would be very close to the magnitude of the beam energy.

At time 400 ms, the power supplies start to turn off in anticipation of switching polarity. However, this does not happen instantaneously, as can be seen on the ramplike transient in Fig. 14. The small steps in the satellite potential at this time can be attributed to the finite fall time of the thruster potentials. Once the thrusters stop emitting, the charge in the satellite is conserved and its potential remains constant while there is no emission. At time 500 ms, the power supplies change polarity and the charging dynamic behavior is mirrored.

B. Single Thruster in Maglev Test Bed

These experiments were performed on the magnetically levitated test bed firing a single thruster. The thruster used in this and all subsequent tests used EMI-BF4 as propellant. In this configuration, C_{HV} was electrically shorted to satellite ground. Because only a single thruster is firing, with no neutralization source, satellite charging will be present. According to the model developed, spacecraft charging cannot continue indefinitely. When the satellite potential is similar to the thruster potential, the emitted and return currents become identical, and the satellite stops charging. The results of a typical test are shown in Fig. 10a.

Notice that the thruster-voltage trace is inverted and the emitted current is multiplied by 10, for visualization purposes. At the beginning of the test, a positive voltage is applied to the thruster; therefore, positive current is emitted. The satellite is then left with excess negative charge, which translates to a negative satellite potential. Because of the extremely low self-capacitance of the

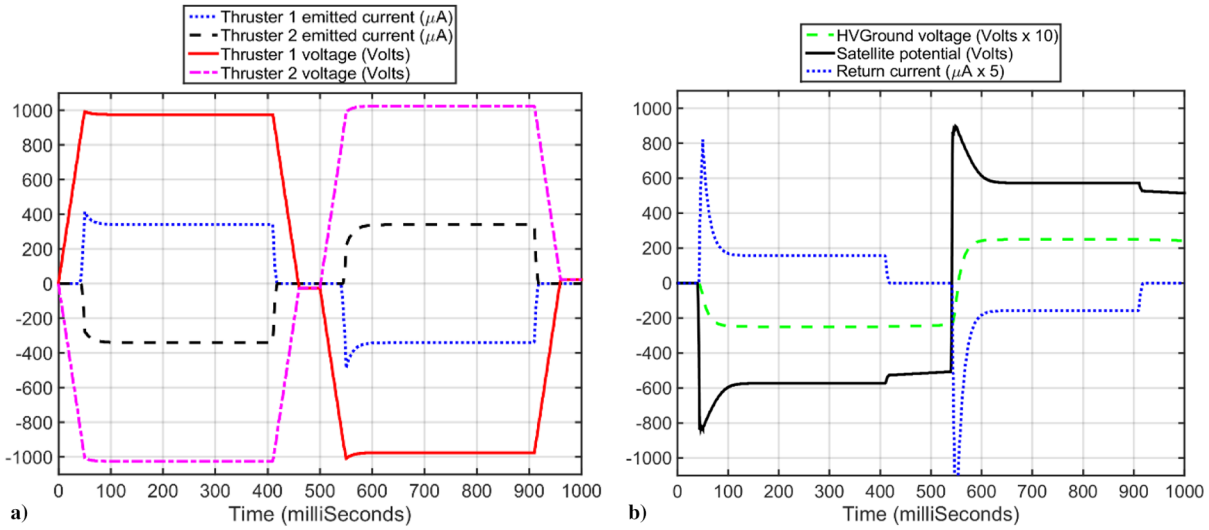

Fig. 14 Simulation of relevant voltages and currents of electrosprays firing in a bipolar configuration: a) relevant thruster variables; and b) satellite potential, return current, and HV_{Ground}.

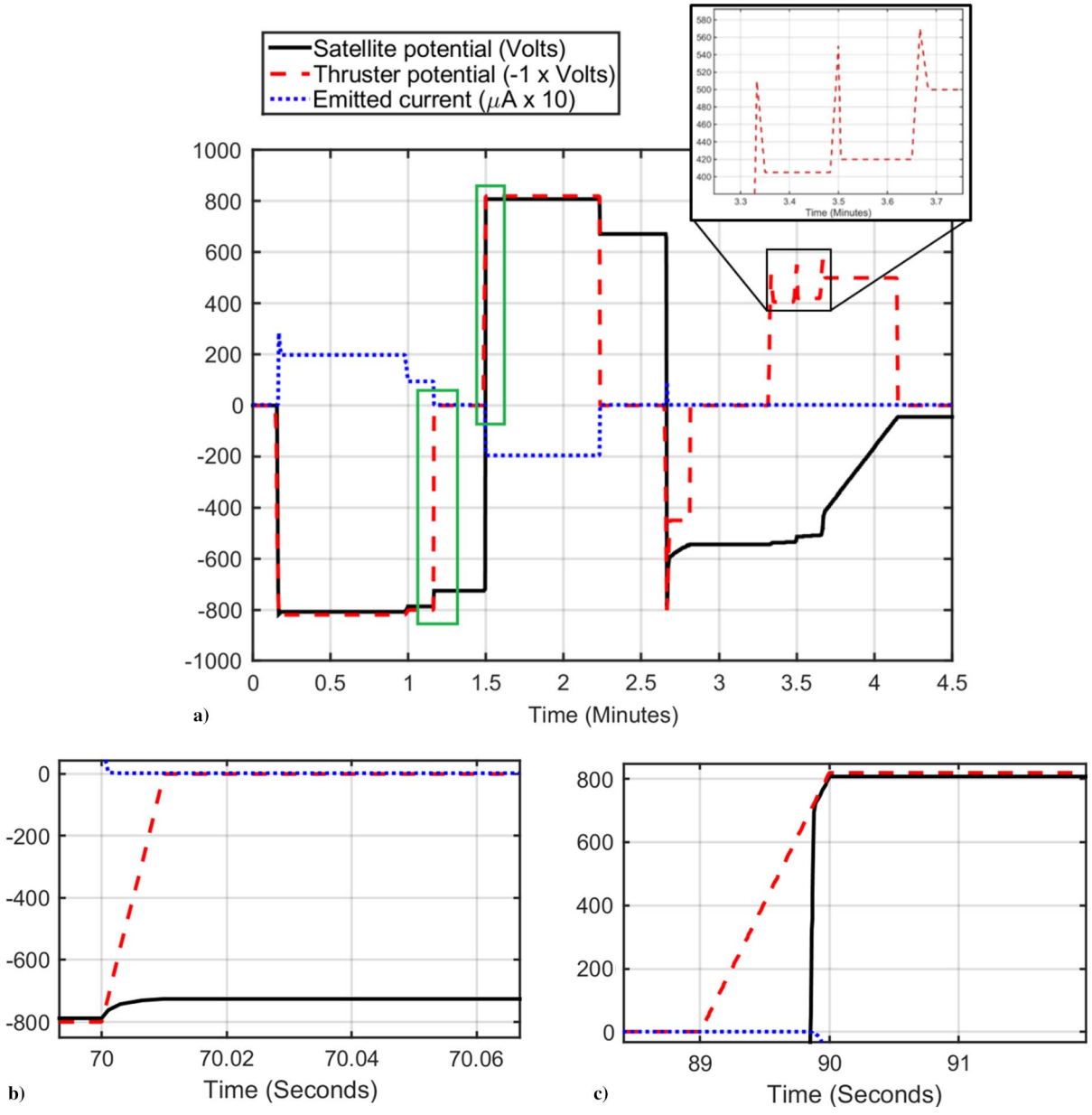

Fig. 15 Re-creation of results of single-thruster test in maglev test bed by simulation: a) entire simulation; and b–c) transient details of the leftmost and rightmost boxes of a), respectively.

satellite (estimated to be 10 pF using a spherical geometry), this charging occurs within 2 ms or less with the microampere emitted current. The satellite-potential magnitude follows the thruster-voltage magnitude and does not exceed it. At time 50 s, the thruster voltage is +850 V and the satellite potential is −843 V. The emitted-current spikes seen at the beginning of every voltage set-point change can be attributed to a fast overshoot of the thruster potential induced by the nonideal PPU voltage controller. The high-voltage monitor circuitry of the PPU is filtered using an RC filter; therefore, some lag is expected between the actual voltage being applied to the thruster and the reported voltage. This explains the lag of the satellite potential with respect to the thruster potential, Fig. 10c. The maximum thruster-voltage fall time was measured to be 5 s, whereas the maximum rise time was 4 s.

When the thruster voltage is turned off, time 70 s, the charge on the satellite is lost and the potential of the satellite reaches zero volts. Notice that, in the absence of secondary current sources, the satellite should have retained its charge. The charge-loss behavior is only seen when emitting positive ions and at currents above 30 μA. It is hypothesized that positively charged secondary particle emissions generated by the ion beam colliding with the chamber wall could be the source of these external currents. Expelled secondary electrons generated by the collision of positive ions that return to the satellite could also account for this external current source.

At time 90 s, the voltage is reversed to a negative polarity and the thruster starts emitting negative ions. The satellite charges rapidly to the positive-emission potential, and stabilizes. At time 110 s, the thruster potential is −831 V and the satellite potential is +828 V. When the voltage is turned off (time 130 s), due to the finite turnoff time, as can be seen in Fig. 10b, the satellite potential follows the voltage applied to the thruster until the thruster stops emitting completely. Notice that, in this polarity, the charge on the satellite is not completely lost and it remains with a +604 V potential after firing.

As previously explained, the picofarad self-capacitance of the satellite makes any thruster-induced charging practically instantaneous with respect to the acquisition-system sampling rate. Therefore, the satellite-potential changes are seen as steps. Charging processes would take longer if very low currents are fired from the thrusters (exponential section of the *I-V* curve). This opens the possibility to explore some of the charging dynamics with the same experimental setup. Beginning at time 160 s, in Fig. 10a, a positive voltage of 500 V is applied to the thruster and the overshoot of the thruster voltage quickly charged the satellite negatively to −605 V. The voltage is turned off and the satellite potential remains constant. Because the voltages are low, the emitted currents are also low, and the charge-loss behavior described previously is not seen.

At time 200 s, −400 V is applied to the thruster and increased slowly until the satellite potential begins to change. At time 215 s, while applying around −500 V, the thruster is emitting such a small current that the charging behavior is slow enough to be clearly resolved by the instrumentation, a nearly linear ramp in this case. The current measurement circuitry in the PPU is not able to detect the small emitted current. However, given the estimated capacitive properties of the levitated satellite and assuming stable emission at these low voltages, it was calculated that the thruster was emitting 133 pA of current during this time.

To validate the model explained in Sec. II, a test with a single thruster was simulated. The simulation, shown in Fig. 15, was performed using similar voltage profiles as the previously described experiment. The self-capacitance of the satellite was estimated to be 10 pF. The simulation parameters are identical to those in Table 2 except for V_{str}, which was set to 878 V.

Notice the resemblance of the simulation results with that of the experimental test of Fig. 10a. However, due to the absence of secondary current sources in the model, the simulation does not capture the charge-loss anomaly described earlier.

C. Evidence of the Return Current

The PPU electronics are able to monitor the current collected by the extractors, which is reported as intercepted current. When the satellite is levitating in the test bed, it is able to charge and, therefore, the return current could be measured. If the satellite is not levitating and is in contact with the grounded test-bed frame, the return current should be zero.

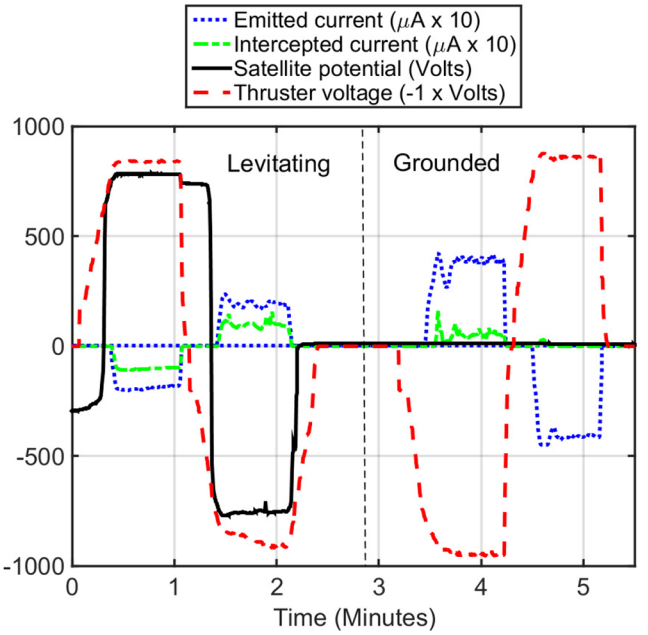

Fig. 16 Evidence of return current while firing an electrospray thruster in the maglev tested.

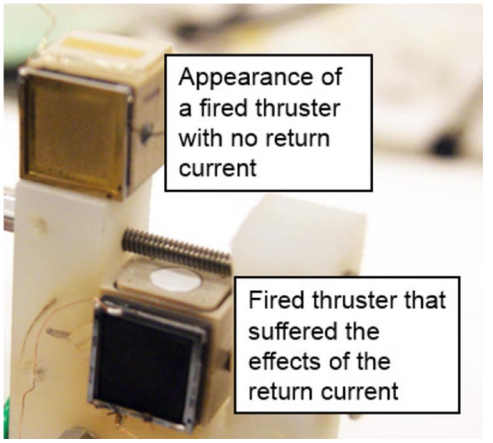

Fig. 17 Effects of the return current on the extractor.

To quantify the difference in collected currents between these two situations, a single-thruster experiment was performed using the same setup as described previously. The results of the test are shown in Fig. 16. The thruster-voltage trace is inverted to help visualization. At the beginning of the experiment, the satellite is levitating, therefore, electrically isolated. At minute 0.2, the thruster is fired with a negative polarity, which positively charged the satellite. The interception current is a fixed fraction of the emitted current, around 50%. When the voltage is turned off, at minute 1.1, the satellite potential follows the thruster potential until the startup threshold is reached. For this particular thruster, the startup voltage was around 780 V. The thruster is then fired in the opposite polarity with similar results as before, from minute 1.3 to 2.5. Notice the charge loss after turning the thruster off, an effect discussed previously. At minute 2.7, marked with a vertical dashed line, the levitation controller is turned off, and the satellite drops and contacts the grounded structure of the test bed. Once more, with the satellite grounded, a positive voltage is applied to the thruster. Positive current is then ejected (around 40 μA at 900 V). When

Table 3 Parameters used for simulation

	Parameter	Value	Units
T_1	V_{str}	915	V
	A	1.075×10^{-24}	V^{-1}
	B	1.173	$V^{-1/2}$
	R	430×10^6	Ω^2
	β	1.4	%
T_2	V_{str}	900	V
	A	1.075×10^{-24}	V^{-1}
	B	1.173	$V^{-1/2}$
	R	430×10^6	Ω^2
	β	1	%
	C_{SC}	10	pF
	C_{HV}	1	nF

the satellite is grounded, the interception current is less than 10%. The thruster is then fired in the negative polarity, in which the interception fraction is close to 1%.

When the satellite is levitating, the return current limits the satellite potential to a value no higher than the thruster potential. When the ions return to the satellite, a significant portion of them hit the extractor, depositing their charge. The returning ions are then measured as an abnormally high interception current, up to 50% in the levitated case. At that point, the monitoring circuitry is reporting the interception current plus the return current. If the satellite is grounded, there is no charging, therefore, no return current, and the monitoring circuitry reports only the nominal interception current.

Returning ions, besides providing neutralization, modify the optical properties of surfaces they impact. In this test, a significant portion of the returning ions was colliding with the extractor. After hours of continuous firing in this configuration, the gold coating on the extractor was significantly discolored; see Fig. 17. Severe discolorations are not present on thrusters that are fired in a grounded scheme, even if they fire for hundreds of hours.

D. Bipolar Configuration

The more realistic scenario of bipolar operation was explored in the maglev test bed. The schematic of the setup used in this experiment can be seen in Fig. 9. Charge balancing is achieved by the operation of two thrusters firing in opposite polarities. The thrusters were mounted on the satellite as to fire in different directions to maximize torque. The results are summarized in Fig. 18. The parameters used for the simulation are shown in Table 3. Notice that the emitted currents are multiplied by a factor of 10.

The thrusters were fired using a high-voltage square-wave profile that switched polarity every 30 s, similar to the waveform used on the simulation shown in Fig. 14. The satellite potential remained within a ± 200 V range during bipolar emission. Thanks to the self-regulating mechanism of the floating power supply, during emission, the emitted currents differ by less than 0.9 μA as reported by the PPU

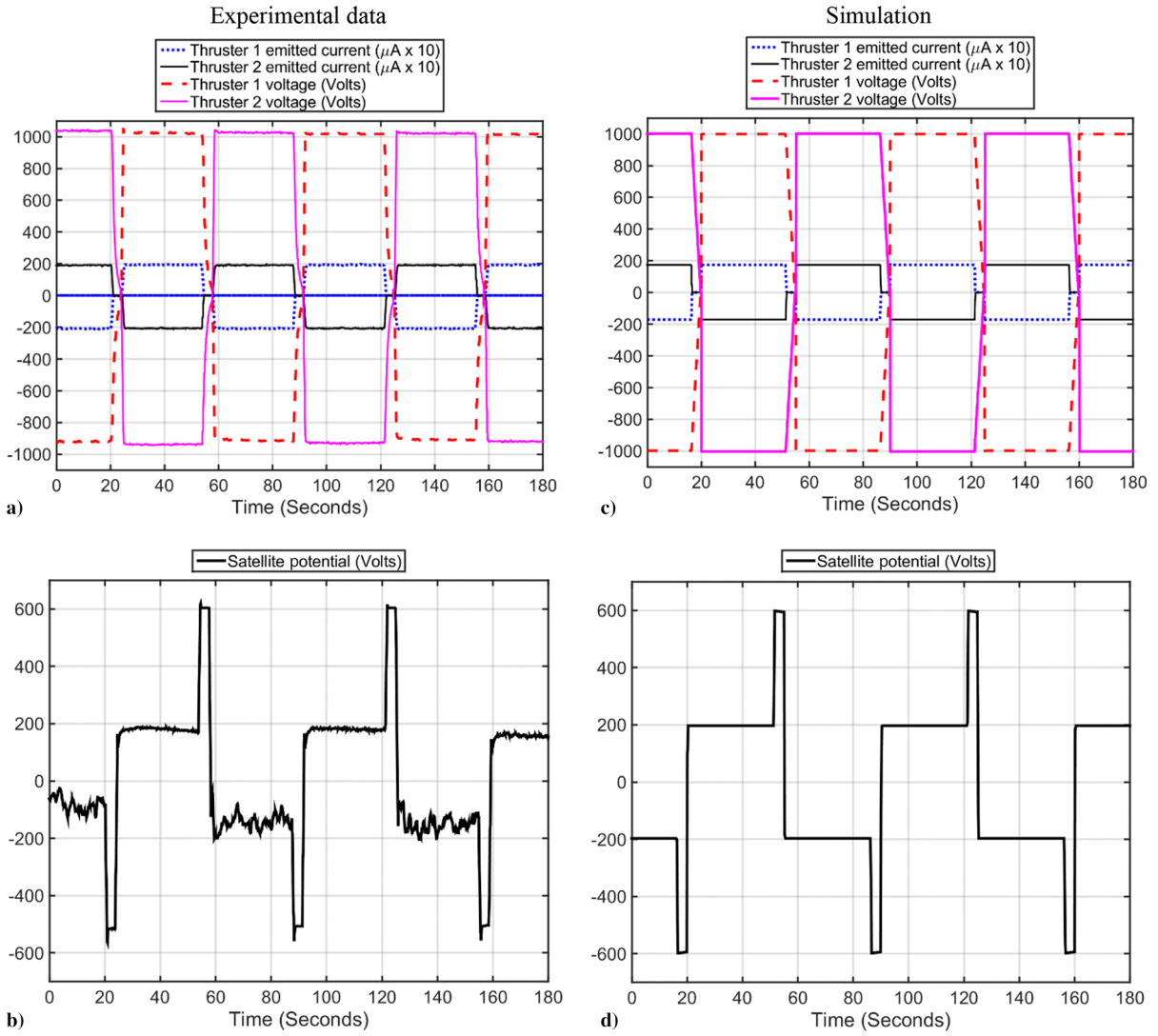

Fig. 18 Experiment and simulation results of firing electrospray thrusters in the bipolar configuration: a–b) measured thruster variables and measured satellite potential, respectively; c–d) simulated thruster variables and simulated satellite potential, respectively.

telemetry. Assuming that both emitted currents are identical during stable emission, the only reason why the satellite charges during each alternation cycle is due to a difference in interception fractions. Any charging due to the transient, in which C_{HV} charges, is mitigated by the return current. Between times 27 and 55 s, T_1 is emitting positive ions, whereas T_2 emits negative ions. The satellite potential at that time is positive; therefore, the extractors must be collecting a net positive current. It can be inferred that T_1 has a higher interception fraction than T_2.

The satellite potential during bipolar emission has a more dynamic behavior compared with the single-thruster cases, especially when thruster T_1 emits negative current. Whenever the power supplies turn off, for example at time 20 s, the charge on the satellite jumps to a higher potential and remains constant. This jump in potential can be attributed to the short, but finite, time it takes the thruster potential to fall to zero and the differences of startup voltage between thrusters. The turnoff transient of the power supply can be seen in Fig. 10a. While the thruster voltages are falling, the startup voltage of T_1 is reached first and transitions to the low-current exponential profile. At that instant, T_2 is still emitting a significant amount of positive ions, which rapidly force the satellite potential to −500 V. Shortly after, the potential across T_2 reaches a point where it stops emitting completely. At this time, because there is no significant emission, the potential of the satellite remains constant until the thrusters are activated again. It can then be concluded that, for this test, T_2 had a slightly lower startup voltage than T_1. At time 90 s, the thruster voltages are reduced, the polarity of the power supply is flipped, and the satellite potential reaches a new equilibrium state with a negative polarity.

VI. Conclusions

The results obtained in simulations and experiments demonstrate that charge balancing with heavy ion species is indeed possible. There are two key passive mechanisms that allow this: the floating power supply and the return current. Allowing the thruster high-voltage power supply to float with respect to the satellite ground ensures that the emitted currents from two thrusters firing in the bipolar configuration become symmetric. The timescale to reach this equilibrium depends proportionally on the capacitance of C_{HV}. This effect can be seen in the results from Fig. 14. The maglev tests presented in Figs. 10 and 16 make the presence of the return current evident. From these tests, it can be concluded that the satellite potential will never exceed the thruster potential.

Another property of electrospray thrusters can be extracted from Fig. 16. Any charge on the satellite would not modify the potential difference between the thruster emitter tips and its extractor. In other words, the amount of emitted current from an electrospray thruster does not depend on the satellite potential. Although the emitted current might not be affected by the satellite potential, the net thrust produced certainly is, as shown in Sec. III. It is then beneficial to operate within a small satellite-potential range to maximize thrust in the bipolar configuration. Finally, results from Fig. 18 show that the charge in the satellite does not increase indefinitely. This is due to the return current counteracting the difference in intercepted currents. In consequence, the satellite potential at which an equilibrium is reached depends on the difference of intercepted currents and the energy distribution of the ion beams. This allows the electrical model to precisely predict the steady-state charging levels of a satellite from the emission and interception properties of specific thruster devices.

There are several behaviors on these tests that need further explanation.

In Fig. 10, the sudden loss of charge at time 1.1 min is abnormal. Positively charged secondary particles generated in the vacuum chamber due to ion collisions with the wall or secondary electrons generated when the return current collides with the satellite seem like plausible explanations. However, these hypotheses require further work before confirmation. The dynamic response of the satellite potential shown in Fig. 18 could be explained by changes in the operational modes of the thrusters. The capacitances involved, C_{SC} and C_{HV}, are small, but they do not allow instantaneous changes in potential. The time delay induced by these capacitors could lead to fast oscillations on the emitted currents and, therefore, on the satellite potential. Further experimentation is needed to verify this hypothesis.

A more complete thruster model would include current sources due to the plasma environment, radiation, and secondary particles, as explained in Sec. II. Further model validating under such conditions could come from actual experiments in space or at least in a more relevant environment in the laboratory.

Acknowledgments

This work was supported by NASA through contract number NNL13AA12C under NASA's Game Changing Development program of the Space Technology Mission Directorate. Fernando Mier-Hicks thanks Mexico's Consejo Nacional de Ciencia y Tecnologia for scholarship support.

References

[1] Gamero-Castaño, M., and Fernández de la Mora, J., "Mechanisms of Electrospray Ionization of Singly and Multiply Charged Salt Clusters," *Analytica Chimica Acta*, Vol. 406, No. 1, 2000, pp. 67–91. doi:10.1016/S0003-2670(99)00596-6

[2] Fernández de la Mora, J., "The Fluid Dynamics of Taylor Cones," *Annual Review of Fluid Mechanics*, Vol. 39, No. 1, 2007, pp. 217–243. doi:10.1146/annurev.fluid.39.050905.110159

[3] Legge, R., and Lozano, P., "Electrospray Propulsion Based on Emitters Microfabricated in Porous Metals," *Journal of Propulsion and Power*, Vol. 27, No. 2, 2011, pp. 485–495. doi:10.2514/1.50037

[4] Dandavino, S., Ataman, C., Chakraborty, S., Shea, H., Ryan, C., and Stark, J., "Design and Fabrication of the Thruster Heads for the MicroThrust MEMS Electrospray Propulsion System," *33rd International Electric Propulstion Conference*, IEPC Paper 2013-127, Oct. 2013.

[5] Krejci, D., Mier-Hicks, F. T., Thomas, R., and Haag, T., "Emission Characteristics of Passively Fed Electrospray Microthrusters with Propellant Reservoirs," *Journal of Spacecraft and Rockets* (to be Submitted).

[6] Deng, W., Klemic, J. F., Li, X., Reed, M. A., and Gomez, A., "Increase of Electrospray Throughput Using Multiplexed Microfabricated Sources for the Scalable Generation of Monodisperse Droplets," *Journal of Aerosol Science*, Vol. 37, No. 6, 2006, pp. 696–714. doi:10.1016/j.jaerosci.2005.05.011

[7] Alexander, M. S., Stark, J., Smith, K. L., Stevens, B., and Kent, B., "Electrospray Performance of Microfabricated Colloid Thruster Arrays," *Journal of Propulsion and Power*, Vol. 22, No. 3, 2006, pp. 620–627. doi:10.2514/1.15190

[8] Chu, E., and Goebel, D. M., "High-Current Lanthanum Hexaboride Hollow Cathode for 10-to-50-kW Hall Thrusters," *IEEE Transactions on Plasma Science*, Vol. 40, No. 9, 2012, pp. 2133–2144. doi:10.1109/TPS.2012.2206832

[9] Goebel, D. M., Watkins, R. M., and Jameson, K. K., "LaB6 Hollow Cathodes for Ion and Hall Thrusters," *Journal of Propulsion and Power*, Vol. 23, No. 3, 2007, pp. 552–558. doi:10.2514/1.25475

[10] Lozano, P., and Martínez-Sánchez, M., "Ionic Liquid Ion Sources: Suppression of Electrochemical Reactions Using Voltage Alternation," *Journal of Colloid and Interface Science*, Vol. 280, No. 1, 2004, pp. 149–154. doi:10.1016/j.jcis.2004.07.037

[11] Lozano, P., and Martínez-Sánchez, M., "Ionic Liquid Ion Sources: Characterization of Externally Wetted Emitters," *Journal of Colloid and Interface Science*, Vol. 282, No. 2, 2005, pp. 415–421. doi:10.1016/j.jcis.2004.08.132

[12] Lozano, P., Glassand, B., and Martinez-Sanchez, M., "Performance Characteristics of a Linear Ionic Liquid Electrospray Thruster," *29th International Electric Propulsion Conference*, IEPC Paper 2005-192, Oct. 2005.

[13] Lozano, P., and Martinez-Sanchez, M., "Efficiency Estimation of EMI-BF4 Ionic Liquid Electrospray Thrusters," *41st AIAA/ASME/SAE/ASEE Joint Propulsion Conference and Exhibit*, AIAA, Reston, VA, July 2005. doi:10.2514/6.2005-4388

[14] Hastings, D., and Garrett, H., *Spacecraft–Environment Interactions*, Cambridge Univ. Press, Cambridge, U.K., 1996, p. 146. doi:10.1017/CBO9780511525032

[15] Anon., "Low Earth Orbit Spacecraft Charging Design Handbook," NASA-HDBK-4006, 2007.

[16] Iribarne, J. V., and Thomson, B. A., "On the Evaporation of Small Ions from Charged Droplets," *Journal of Chemical Physics*, Vol. 64, No. 6, 1976, pp. 2287–2294. doi:10.1063/1.432536

[17] Guerra-Garcia, C., Krejci, D., and Lozano, P., "Spatial Uniformity of the Current Emitted by an Array of Passively Fed Electrospray Porous Emitters," *Journal of Physics D: Applied Physics*, Vol. 49, No. 11, 2016, Paper 115503. doi:10.1088/0022-3727/49/11/115503

[18] Courtney, D. G., "Ionic Liquid Ion Source Emitter Arrays Fabricated on Bulk Porous Substrates for Spacecraft Propulsion," Ph.D. Thesis, Dept. of Aeronautics and Astronautics, Massachusetts Institute of Technology, Cambridge, MA, 2011.

[19] Courtney, D. G., Dandavino, S., and Shea, H., "Comparing Direct and Indirect Thrust Measurements from Passively Fed Ionic Electrospray Thrusters," *Journal of Propulsion and Power*, Vol. 32, No. 2, 2016, pp. 392–407. doi:10.2514/1.B35836

[20] Courtney, D. G., and Shea, H., "Fragmentation in Time-of-Flight Spectrometry-Based Calculations of Ionic Electrospray Thruster Performance," *Journal of Propulsion and Power*, Vol. 31, No. 5, 2015, pp. 1500–1504. doi:10.2514/1.B35837

[21] Mier-Hicks, F. L., and Lozano, P., "Thrust Measurements of Ion Electrospray Thrusters Using a CubeSat Compatible Magnetically Levitated Thrust Balance," *Joint Conference of 30th International Symposium on Space Technology and Science and 34th International Electric Propulsion Conference and 6th Nano-Satellite Symposium*, IEPC Paper 2015-148, July 2015.

[22] Mier-Hicks, F., "Characterization on a Magnetically Levitated Testbed for Electrospray Propulsion Systems," M.S. Thesis, Dept. of Aeronautics and Astronautics, Massachusetts Institute of Technology, Cambridge, MA, 2014.

[23] Mier-Hicks, F., Perna, L., Coffman, C., and Lozano, P., "Characterization of a CubeSat Compatible Magnetically Levitated Thrust Balance for Electrospray Propulsion Systems," *49th AIAA/ASME/SAE/ASEE Joint Propulsion Conference*, AIAA Paper 2013-3879, July 2013. doi:10.2514/6.2013-3879

G. G. Spanjers
Associate Editor